Engineering Fracture Mechanics Vol. 19. No. 4. pp. 633–642. 1984
Printed in Great Britain.

0013-7944/84 $3.00 + .00
Pergamon Press Ltd.

THE ASSESSMENT OF DEFECTS IN STRUCTURES OF STRAIN HARDENING MATERIAL

R. A. AINSWORTH
Central Electricity Generating Board, Berkeley Nuclear Laboratories, Berkeley, Gloucestershire, England

Abstract—J-estimation procedures based on finite-element solutions are expressed in terms of the material stress–strain curve by using reference stress techniques common in creep analysis. The result is an exact representation of the estimation procedures for materials which strain harden according to the simple power law used in the finite-element caclulations. For other materials, it is shown that an appropriate definition of the reference stress reduces the dependence of the results on the accuracy to which the strain hardening can be described by a simple power law. The resulting reference stress based estimation procedure is used to derive a failure assessment curve for use with the CEGB failure assessment route. Comparison is made with the modified failure assessment curve recently suggested by Milne and the implications of the results for defect assessments are discussed.

1. INTRODUCTION

IN POST-YIELD fracture mechanics (PYFM) experimental and analytical work has demonstrated that the onset of crack growth and subsequent small amounts of crack extension can be described by parameters such as J and crack opening displacement. The finite-element method enables these parameters to be evaluated and hence the defect tolerance of a structure to be assessed. However, the finite-element method requires considerable computational effort for complex geometries and consequently a number of simplified PYFM methods have also been developed. These include the CEGB failure assessment route [1], the COD design curve [2], the J-design curve [3] and J-estimation schemes [4]. Burdekin, *et al.* [5] compared these methods by performing calculations for several geometries using material properties for an A533B steel. Although some differences in the results occurred due to different treatments of residual stresses and different choices of yield or flow strength, they found broad agreement between the various approaches.

Much of the development work on the above defect assessment procedures has been based on materials such as A533B steel and some weld metals for which the ratio of ultimate strength to yield strength is low. In these materials the strain-hardening properties can be adequately described by power-law hardening (as in the J-estimation schemes) or by a flow stress (for example, the mean of ultimate and yield strengths as in the CEGB failure assessment route). However, Milne [6] has recently shown that neither of these approaches is satisfactory for describing the strain-hardening response of materials in which the yield and ultimate strengths are significantly different. A simple power law does not accurately describe the stress–strain curve over the wide range of stress and strain between yield and ultimate in such materials so making the J-estimation schemes difficult to use. Equally, the use of a flow stress in the CEGB failure assessment route is inadequate and Milne [6] suggests that an additional dependence on the ratio of ultimate to yield strength should be included. The present paper considers how both the J estimation schemes and the CEGB failure assessment route can be modified to deal with strain-hardening materials, and how the two methods are related to each other.

2. ELASTIC–PLASTIC ESTIMATION SCHEME FOR J

2.1 *Basic estimation scheme of Kumar and Shih*

Consider a material for which the uniaxial stress strain ($\sigma - \epsilon$) curve may be described by:

$$\epsilon/\epsilon_0 = \sigma/\sigma_0 + \alpha(\sigma/\sigma_0)^n \tag{1}$$

where σ_0, ϵ_0, α and n are constants. The constant σ_0 is a yield or proof stress and it is often convenient to choose $\epsilon_0 = \sigma_0/E$ where E is Young's modulus. For a material obeying eqn (1), Kumar and Shih [4] suggest that in a structure having a crack of length a in section width w, the value of J at an applied load P may be estimated from

$$J = K^2(a_e)/E' + \alpha\sigma_0\epsilon_0 c\, h_1(a/w, n)(P/P_0)^{n+1}. \tag{2}$$

The first term in eqn (2) corresponds to essentially elastic behaviour with K the elastic stress intensity

factor, a_e an effective crack length defined below, $E' = E$ in plane stress and $E' = E/(1-\nu^2)$, where ν is Poisson's ratio, in plane strain. The second term is obtained from fully plastic solutions which by normalisation in terms of a characteristic dimension c (for example, the uncracked ligament $w-a$) and a characteristic load P_0 (for example, the limit load defined for a rigid plastic material of yield strength σ_0) are represented by the non-dimensional functions h_1, tabulated for different geometries by a number of authors (for example [4, 7–9]). The modified crack length a_e is given in [4] as

$$a_e = a + \frac{1}{\beta\pi}\frac{(n-1)}{(n+1)}\left(\frac{K}{\sigma_0}\right)^2 \frac{1}{[1+(P/P_0)^2]} \tag{3}$$

where $\beta = 2$ for plane stress, $\beta = 6$ for plane strain and $K = K(a)$. This modification essentially provides a plastic zone correction which is arranged to have a reduced effect at higher loads when plasticity contributions are given by the second term in eqn (2).

2.2 *Estimation scheme in terms of the strain at a reference stress*

Although eqn (2) is straightforward to use given a geometry for which h_1 is defined, there are some difficulties when it is applied in practice. One of these is the difficulty of fitting eqn (1) to stress–strain curves of strongly work hardening materials [6]; the constants α, n which give a good fit at low strains may be significantly different from those which give a good fit at high strains. Because of the power-law dependence of eqn (2) on n, large differences in calculated values of J can arise from different fits of eqn (1) to the stress–strain curve. In this paper it is suggested that such curve-fitting errors may be reduced by adopting reference stress techniques commonly used in creep analysis (see, for example [10]). Defining the reference stress by:

$$\sigma_{\text{ref}} = (P/P_0)\sigma_0 \tag{4}$$

eqn (2) becomes

$$J = K^2(a_e)/E' + ch_1(a/w, n)\,\sigma_{\text{ref}}\,(\epsilon_{\text{ref}} - \sigma_{\text{ref}}\,\epsilon_0/\sigma_0) \tag{5}$$

where ϵ_{ref} is, from eqn (1), the uniaxial strain corresponding to the stress σ_{ref}. Equation (5) is an exact representation of eqn (2) for materials which follow eqn (1). For other materials, J may be evaluated from eqn (5) using the stress–strain curve directly, thus removing the power-law dependence of eqn (2) on n.

2.3 *Choice of normalising load used to define the reference stress*

Since the parameter h_1 depends on n, eqn (5) is still influenced by the value of n used to describe the stress–strain curve. However, in representing finite-element results in terms of tabulated values h_1, it is apparent from eqn (2) that h_1 depends on the normalising load P_0 according to

$$h_1/P_0^{n+1} = \text{const.} \tag{6}$$

The essence of the reference stress method is to choose P_0 (i.e. to define σ_{ref} through eqn (4)) so as to minimise the dependence of h_1 on n. From eqn (6), if $\log(h_1)$ varies linearly with n for any given value of P_0, then h_1 can be made independent of n by an alternative choice of P_0.

The dependence of h_1 on the choice of P_0 is illustrated in Fig. 1 for the specific example of a compact tension specimen in plane strain with $a/w = 1/2$. The values of h_1 are taken from [4]. It can be seen that h_1 varies strongly with n for the value $P_0 = 0.118\,Bw\sigma_0$ used in [4] and, for example, $h_1(1)/h_1(20) \simeq 15$. By setting $P_0 = 0.136\,Bw\sigma_0$ the variation of $h_1(n)$ is minimised in the range $n \leqslant 20$ as shown in Fig. 1. Results for two other normalising loads are also shown: the load $P_0 = 0.134\,Bw\sigma_0$ gives a variation of h_1 which is asymptotic to a constant value at large n; the load $P_0 = 0.129\,Bw\sigma_0$ is the limit load given by Ewing (see [11]) and Rice (see [4]). Since the material behaviour approximates to elastic-perfectly plastic for large n, it is perhaps surprising that these last two loads are not equal. However, the differences in P_0 are less than 5% and may be due to errors in the finite-element solutions on which h_1 is based, uncertainties in the limit load, or simply that the value $n = 20$ is not sufficiently large for a true asymptote to be reached. Given the uncertainties in finite-element solutions, the data in Fig. 1 can

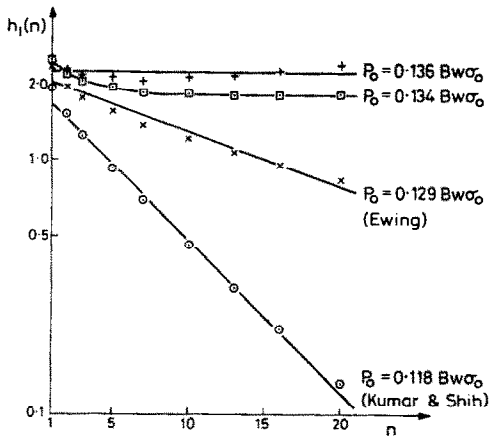

Fig. 1.

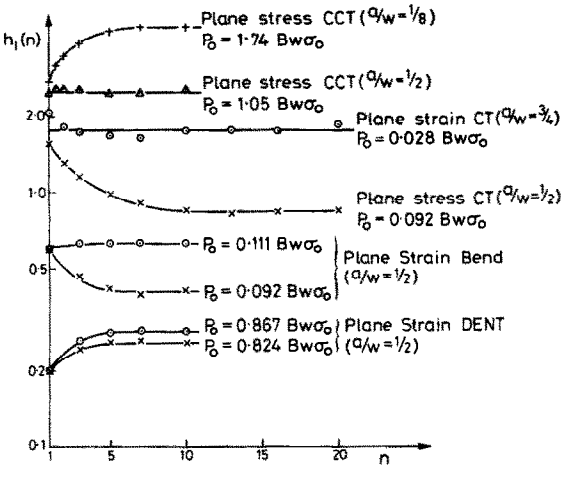

Fig. 2.

Fig. 1. Variation of h_1 with n for a compact tension specimen ($a/w = \frac{1}{2}$) in plane strain.

Fig. 2. Variation of normalised J values with hardening exponent.

probably be represented sufficiently accurately by a single value of h_1 over the entire range $n \leqslant 20$, and with the reference stress defined by eqn (4) with $P_0 = 0.136\ Bw\sigma_0$.

Some further examples are shown in Fig. 2 and given in Table 1. The values of P_0 have been chosen to give a minimum variation with n either over the full range of n, or where there is an obvious systematic variation only over a limited range at higher n as indicated in Table 1. In order to illustrate the accuracy of the solutions, for the DENT and bend specimens, Table 1 and Fig. 2 include two

Table 1. Normalised load and J values for a range of geometries

Geometry	Plane Stress or Strain	$\frac{a}{w}$	Normalising Range of n	$\frac{\bar{h}_1}{h_1(1)}$	Normalising Load $P_0/Bw\sigma_0$	Limit Load $P_L/Bw\sigma_0$
CT	Strain	3/8	1-20	0.91	0.231	0.221
	Strain	1/2	1-20	0.87	0.136	0.129
	Strain	3/4	1-20	0.89	0.028	0.027
	Stress	1/2	10-20	0.53	0.092	0.089
CCT	Stress	1/8	7-10	1.63	1.74	1.75
	Stress	1/2	1-10	1.02	1.05	1.00
DENT	Strain	1/2	5-10	1.42	0.87	0.81
	Strain	1/2	5-10	1.30	0.82	
BEND	Strain	1/2	5-10	1.05	0.111	0.088
	Strain	1/2	5-10	0.68	0.092	

solutions given in [9], one based on a finite-element displacement method and the other on a stress method. Table 1 is by no means exhaustive and it is worth noting that normalised J functions are not always well behaved in the limit $n \to \infty$ (see, for example, [12]). However, the limit $n \to \infty$ is not a problem as, irrespective of h_1, the estimation scheme for large n leads to rapid variations of J for loads in the neighbourhood of P_0. In the present paper, the particular interest is in strongly work hardening materials which are described by low values of n.

Table 1 includes the mean value ($\bar{h}_1$) of h_1 over the range of n for which P_0 has been chosen to normalise the data. In Table 1, this mean value is compared with the value of $h_1(n = 1)$ and it can be seen that the ratio is generally close to unity. The fully plastic solution for $n = 1$ corresponds to an elastic solution for Poisson's ratio $\nu = 1/2$ so that eqn (5) requires:

$$\mu K^2(a) = c\, h_1(1)\sigma_{\text{ref}}^2 \tag{7}$$

where $\mu = 1$ for plane stress, $\mu = 0.75$ for plane strain and the notation $h_1(1) = h_1(a/w, 1)$ has been adopted. With this substitution and adopting the value of P_0 which gives an essentially constant value ($h_1 = \bar{h}_1$) of h_1 to define the reference stress, eqn (5) becomes.

$$J = K^2(a_e)/E' + (\mu K^2(a)/E)[\bar{h}_1/h_1(1)](E\epsilon_{\text{ref}}/\sigma_{\text{ref}} - 1) \tag{8}$$

where additionally σ_0/ϵ_0 has been set equal to E.

Equation (8) is the representation of the J-estimation schemes proposed in the present paper. For its use, it requires the basic finite-element fully plastic data to be represented by a single ratio $\bar{h}_1/h_1(1)$ and a single load P_0. Clearly for a material which is described by eqn (1) with $\epsilon_0 = \sigma_0/E$, it should give identical results to the original estimation scheme of eqn (2) provided n lies in the appropriate normalising range used to establish P_0 and $\bar{h}_1$. For other materials it is independent of any parametric fit to the stress–strain curve and should be most useful in the cases indentified in [6] where the value of n depends strongly on the range of strain used to fit the power law of eqn (1).

2.4 *Approximate representation of the estimation scheme*

In order for J to be estimated from eqn (2) or eqn (8) it is necessary that finite-element solutions are available to provide the fully plastic results. In practice J solutions are only known for a limited number of, mostly test specimen, geometries so that some geometric idealisation or the generation of further finite-element results is required. The results of the previous sub-section suggest an alternative approximate approach. It has already been noted that the ratio $\bar{h}_1/h_1(1)$ is close to unity for the range of geometries considered. Equation (8) may, therefore, be simplified by adopting

$$\bar{h}_1 \simeq h_1(1).$$

It is worth noting that at large n where the mean value $\bar{h}_1$ is likely to differ most from $h_1(1)$, the accuracy of this approximation is least important as errors correspond to small differences in applied loading.

Table 1 includes values of limit load, P_L, taken from the compendium of Haigh and Richards [11] for test specimens (for the CT specimen in plane stress they only give a limit load based on the Tresca yield criterion; the value in Table 1 has been obtained using the Mises expression given in their source reference. All other values in Table 1 have been obtained directly from [11]). It can be seen that the limit load P_L is typically 5% lower than P_0. Since limit loads are more widely available (for example, [13]) than fully plastic J solutions a reasonable approach is to replace P_0 by P_L when P_0 is unknown and so eqn (8) becomes finally

$$J = K^2(a)/E'[K^2(a_e)/K^2(a) + (\mu E'/E)(E\epsilon_{\text{ref}}/\sigma_{\text{ref}} - 1)] \tag{9}$$

where

$$\sigma_{\text{ref}} = P\sigma_0/P_L(\sigma_0).$$

The results of Table 1 for test specimens suggest that in applications to components, eqn (9) will typically underestimate the load carrying capacity of a component by 5% in the post-yield fracture

region. Given the alternative of performing a finite element analysis, this does not seem an unreasonable penalty, particularly as finite element solutions for even simple geometries are subject to similar errors (see Table 1).

In defining the modified crack length a_e in eqns (8) and (9) the normalising load P_0 or the limit load P_L should be used. Given the empirical nature of eqn (3) and the closeness of these loads to those used in [4], this does not represent a significant departure from the original estimation scheme.

3. THE CEGB FAILURE ASSESSMENT METHOD

3.1 *Basic method of Harrison* et al.

The CEGB failure assessment method (Harrison *et al.* [1]) uses the non-dimensional load and stress intensity factor parameters K_r and S_r defined by

$$K_r = K/K_c = (K^2/E'J_c)^{1/2} \tag{10}$$

$$S_r = P/P_L(\bar{\sigma}) \tag{11}$$

where K_c is the material toughness and $P_L(\bar{\sigma})$ is the limit load defined for a yield or flow stress $\bar{\sigma}$. The method is depicted in Fig. 3. For a given structure, loading and defect size the two parameters K_r and S_r are evaluated from eqns (10) and (11); if the resulting assessment point (S_r, K_r) lies within the failure line of Fig. 3 the defect is acceptable. In general the failure line depends on geometry but in practice the geometry dependence is found to be small [14] so that a "universal" failure curve may be adopted leading to a very simple method for defect assessments. In [1] the curve adopted was

$$K_r = S_r[(8/\pi^2) \ln \sec (\pi S_r/2)]^{-1/2} \tag{12}$$

with $\bar{\sigma} = 1/2(\sigma_u + \sigma_0)$, where σ_u is the ultimate stress and σ_0 the yield stress, being used in eqn (11). With this definition of $\bar{\sigma}$, eqn (12) provides a satisfactory means of avoiding failure in ferritic steels for a wide range of geometries [15].

3.2 *Modification of Milne for strain hardening*

Milne [6] has recently shown that eqn (12) with S_r defined by a flow stress is not adequate for strongly work hardening materials. On the basis of some experimental data and the J-estimation schemes, primarily for bend specimens, Milne has suggested the failure curve

$$K_r = S_r'[(8/\pi^2) \ln \sec (\pi S_r'/2)]^{-1/2} \tag{13}$$

where

$$S_r' = S_r - (1 - K_r^{1/2})(\sigma_u/\sigma_0 - 1)$$

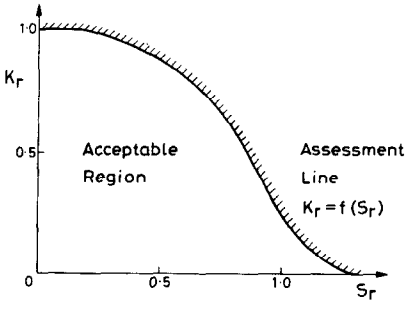

Fig. 3. The failure assessment diagram.

with $\bar{\sigma} = \sigma_0$ being used to define S_r in eqn (11). At small $K_r (\leq 1/2)$, $S_r' \simeq 1$ and eqns (13) simplify to

$$K_r \simeq \left[\frac{\sigma_u/\sigma_0 - S_r}{\sigma_u/\sigma_0 - 1}\right]^2, \quad K_r \leq 1/2. \tag{13a}$$

The formulation of eqn (13) retains the geometry independence and hence the simplicity of the original failure assessment curve. It is discussed further in Section 4 below.

3.3 *Failure assessment curve based on the* J*-estimation scheme*

As an alternative to that given in [6] the present paper derives a failure assessment curve from the reference stress based estimation scheme of Section 2. A failure line for use with the CEGB method may be obtained by setting J, predicted from Section 2, equal to its critical value J_c used in defining K_r in eqn (10). With this substitution the J-estimation method of eqn (8) gives in eqn (10)

$$K_r^{-2} = K^2(a_e)/K^2(a) + (\mu E'/E)[\bar{h}_1/h_1(1)](E\epsilon_{\text{ref}}/\sigma_{\text{ref}} - 1), \tag{14}$$

where $\sigma_{\text{ref}} = P\sigma_0/P_0$. From eqn (11), $\sigma_{\text{ref}} = S_r\sigma_0(P_L/P_0)$ with $\bar{\sigma}$ equal to the yield stress σ_0. In the form of eqn (14), the J-estimation schemes for particular geometries may be plotted as failure curves on the failure assessment diagram. However, because of the geometry dependence, eqn (14) is not particularly useful for general use. The approximate representation of the estimation scheme by eqn (9) does provide a means of obtaining a more generally useful failure curve since combining eqns (9)–(11) leads to

$$K_r = [\lambda E\epsilon_{\text{ref}}/\sigma_{\text{ref}} + (1-\lambda) + \gamma S_r^2/(1+S_r^2)]^{-1/2} \tag{15}$$

with $\bar{\sigma} = \sigma_0$ and $\sigma_{ref} = S_r\sigma_0$. The constant $\lambda = (\mu E'/E)$, i.e. $\lambda = 1$ in plane stress and $\lambda = 0.75/(1-\nu^2)$ in plane strain. The value of γ is defined by the plastic zone correction of eqn (3) and eqn (7) as

$$1 + \gamma\left(\frac{S_r^2}{1+S_r^2}\right) = K^2\left[a + \frac{ch_1(1)}{\mu\beta\pi}\left(\frac{n-1}{n+1}\right)\left(\frac{S_r^2}{1+S_r^2}\right)\right]\Big/K^2(a)$$

which for small corrections to the crack length simplifies to

$$\gamma \simeq \left(\frac{2}{\mu\beta\pi}\right)\left(\frac{n-1}{n+1}\right)ch_1(1)\frac{\partial K/\partial a}{K}. \tag{16}$$

A geometry independent failure curve is obtained from eqn (15) by setting a fixed value for γ. This value is rather arbitrary and the choice used here is $\gamma = 1/2$ which is obtained from eqn (16) for an infinite cracked plate in tension under plane stress conditions with $n \to \infty$. The failure assessment curve proposed in this paper may then be summarised as

$$K_r \leq [E\epsilon_{\text{ref}}/\sigma_{\text{ref}} + 1/2S_r^2/(1+S_r^2)]^{-1/2} \tag{17}$$

and

$$S_r \leq \sigma_u/\sigma_0$$

with

$$\sigma_{\text{ref}} = S_r\sigma_0$$

and

$$S_r = P/P_L(\sigma_0).$$

In eqn (17) the constant value $\lambda = 1$ has been adopted for simplicity; this is exact for plane stress, or plane strain with $\nu = 1/2$. In addition, an upper limit to S_r has been imposed as one aim of the CEGB

method is to avoid plastic collapse and such a limit does not result from the post-yield fracture method using J. Equation (17) differs from eqn (13) as it suggests that the shape of the stress–strain curve rather than simply the ratio σ_u/σ_0 influences fracture. These differences are discussed further in section 4 below where both approaches are compared with experimental and finite-element results. In view of the results of Section 2 the present approach would be expected to lead to errors of typically 5% in load carrying capacity if it were applied to test specimen data in the post-yield region.

4. COMPARISON OF ASSESSMENT PROCEDURES

The various failure assessment lines of eqns (12), (13) and (17) may be conveniently described by the equation

$$K_r = f(S_r) \tag{18}$$

where the function f and the definition of S_r depend on the method adopted. For elastic-perfectly plastic materials ($\sigma_u/\sigma_0 = 1$) eqns (12) and (13) are identical. Setting $\epsilon_{ref} = \sigma_{ref}/E$ for $\sigma_{ref} < \sigma_0$ and ϵ_{ref} unbounded for $\sigma_{ref} = \sigma_0$, eqn (17) gives

$$K_r = [1 + 1/2\, S_r^2/(1 + S_r^2)]^{-1/2}, \quad S_r < 1$$

and K_r falls discontinuously to zero at $S_r = 1$. This is similar to eqn (12) which gives a rapid drop in K_r near $S_r = 1$ ($K_r = 0.54$ at $S_r = 0.99$, $K_r = 0$ at $S_r = 1.0$) and agrees with eqn (12) at small S_r if the fraction 1/2 is replaced by $\pi^2/24$. The difference between 1/2 and $\pi^2/24$ arises from the small difference between the Dugdale solutions [16] for an infinite cracked plate in tension (on which eqn (12) is based) and the first-order plastic zone correction of eqn (3) at small stresses for the same geometry. This agreement between all methods for materials with a low ratio of σ_u/σ_0 is exemplified by Fig. 4 using the stress–strain curve of an A533B steel given in [6]. For consistency S_r has been defined by $S_r = P/P_L(\sigma_0)$ so that eqn (12) has been drawn for S_r replaced by $S_r' = 2S_r\sigma_0/(\sigma_u + \sigma_0)$.

For strain hardening materials the differences between the approaches are typified by Fig. 5(b) which is based on the stress–strain curve of Fig. 5(a) (from [17]). For consistency, S_r has again been defined in terms of the yield strength σ_0 and eqn (12) modified accordingly. Equation (17) has been used with the true stress–strain curve but use of the engineering stress–strain curve makes little significant difference except near the cut-off at $S_r = \sigma_u/\sigma_0$.

It can be seen from Fig. 5(b) that the implications for defect assessments of using various forms of eqn (18) depend on the ratio K_r/S_r. At high K_r/S_r (≥ 1) failure is predicted to occur at values of K close to K_{1c} by all three lines so that differences in predicted load bearing capacity are negligible. At low K_r/S_r (< 0.2) failure is dominated by plastic collapse and the final failure load may be governed by geometric instability rather than by crack tip events. The shape of the assessment line in this region is somewhat arbitrary and it is probably most convenient to limit the diagram by the cut off at $S_r = \sigma_u/\sigma_0$ or perhaps more conservatively by a cut off based on the flow strength. Significant differences exist between the

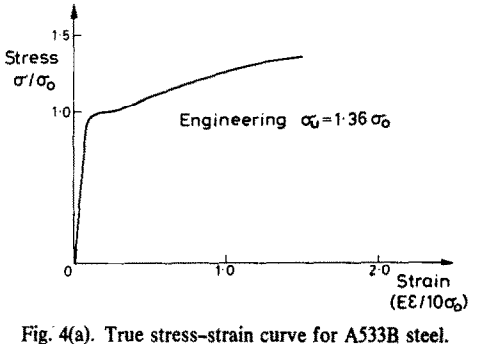

Fig. 4(a). True stress–strain curve for A533B steel.

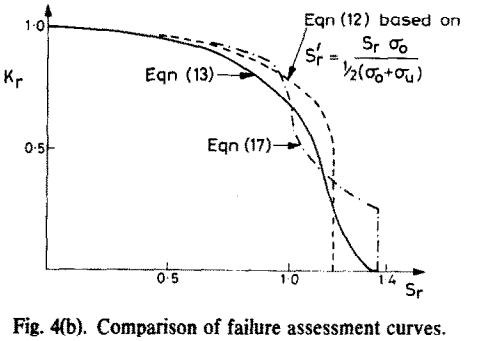

Fig. 4(b). Comparison of failure assessment curves.

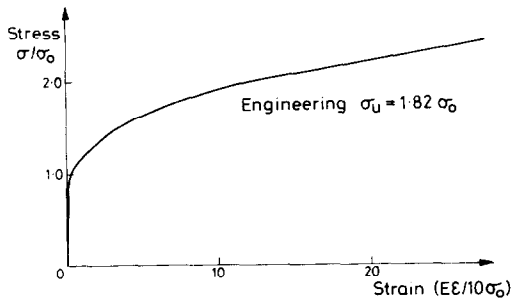

Fig. 5(a). True stress–strain curve for a mild steel.

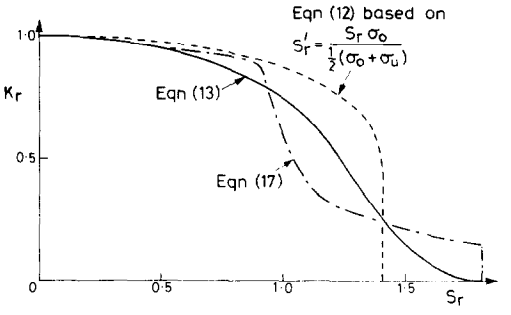

Fig. 5(b). Comparison of failure assessment curves.

curves of Fig. 5(b) at intermediate ratios of K_r/S_r and it is apparent that the original failure assessment curve of eqn (2) based on a flow stress can lead to overestimates of the load-carrying capacity. The curves of eqns (13) and (17) are in closer agreement, but even these differ significantly over a narrow load range. These differences may be understood by comparing eqns (13a) and (17) at a typical value of $K_r \simeq 1/2$ in this range. For this value of K_r, eqn (13a) gives:

$$S_r = 1 + (1 - 1/\sqrt{2})(\sigma_u/\sigma_0 - 1)$$

i.e.

$$\sigma_{\text{ref}} \simeq \sigma_0 + 0.3(\sigma_u - \sigma_0).$$

If the two methods were to agree then eqn (17) would require that the strain at this reference stress is $E\epsilon_{\text{ref}}/\sigma_{\text{ref}} \simeq 4$. This means that the strain at a stress 30% between yield and ultimate is a small multiple of the elastic strain, i.e. that the initial hardening rate is high. The situation is depicted schematically in Fig. 6 for two materials with the same ratio σ_u/σ_0: the approach of Milne given by eqn (13) is probably adequate for materials such as (1) with a high initial hardening rate, but is likely to be unconservative for materials such as (2) which exhibit large strains at stresses not much greater than the yield strength.

4.1 *Comparison with finite-element and experimental data*

For some standard test specimen geometries, J is simply related to the external work (U, say) by a constant which is independent of load (for example, [18]). In these cases eqn (10) becomes

$$U/U^{\text{el}} = K_r^{-2} \tag{19}$$

where U^{el} is the elastic value, i.e. $U^{\text{el}} = 1/2P\Delta^{\text{el}}(P)$ where Δ^{el} is the elastic displacement under the applied load P. Equations (17) and (19) may be combined to obtain the load-displacement behaviour $\Delta(P)$. This is not pursued here, but it is worth noting that failure assessment lines which are independent of geometry imply that for a range of standard test specimens the load–deflection behaviour is independent of geometry when normalised as P/P_0 vs $\Delta/\Delta^{\text{el}}$.

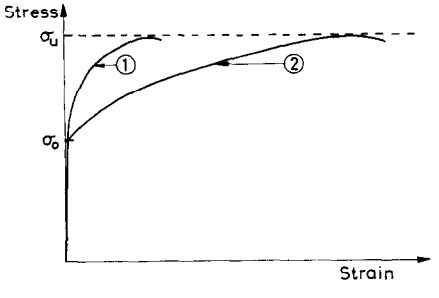

Fig. 6. Schematic material behaviour.

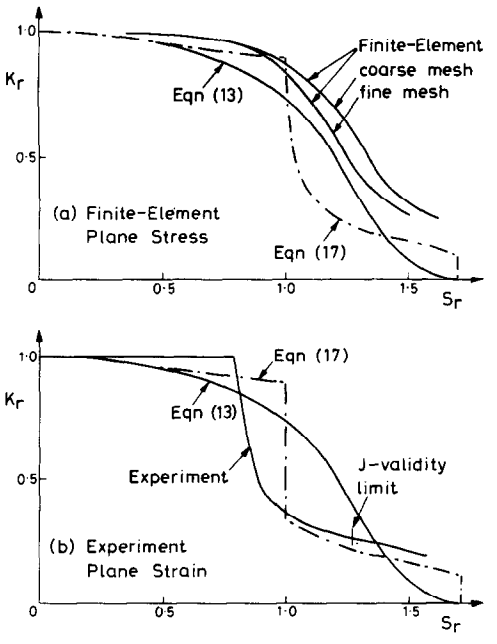

Fig. 7. Representation of bend specimen data from [19] on the failure assessment diagram.

Using eqn (19), load-deflection data from Neale [19] for a three point bend specimen with $a/w = 1/2$ are represented as curves on the failure assessment diagram. The plane stress finite-element results obtained by Neale are compared with eqns (13) and (17) in Fig. 7(a). It can be seen that the results are in better agreement with eqn (13) but that significant differences exist between solutions for different finite-element idealisations. The finite-element results also tend to overestimate the collapse load based on the ultimate strength (see Fig. 9 of [19]), and so are likely to be slightly non-conservative at higher S_r.

Neale also carried out an experimental programme and his results for a specimen without side-grooves are shown in Fig. 7(b). The maximum load achieved in the test was close to the plane strain limit load given in [11] and so this load has been used to normalise the experimental results. The values of K_r derived from eqn (19) at high S_r should be treated with caution as the corresponding values of J violate the criteria which enable valid J values to be obtained from the load-deflection response (the validity limit is indicated in Fig. 7). The carbon–manganese steel used in the test exhibited discontinuous behaviour at the yield stress and this is reflected in the discontinuity in eqn (19) in Fig. 7(b); the finite-element calculations used a multilinear representation which smoothed out the stress–strain curve resulting in the smooth curve for eqn (17) in Fig. 7(a). It can be seen from Fig. 7(b) that the experimental results follow the trend predicted by eqn (17) and are in close agreement with the curve of eqn (17) beyond $S_r = 1$. Differences exist between the experimental results and eqn (17) at loads in the range $S_r = 0.8 - 1.0$ and the differences between the experimental curve and eqn (13) are very marked in this region. Neale [19] found that the experimental load-deflection response was reasonably well described by the plane stress finite-element solution for this load range even though the maximum load achieved in the test was close to the plane strain collapse load which is some 40% higher than the plane stress collapse load. This is rather surprising and it may be that the experimentally observed departure from essentially elastic behaviour at low loads is simply a result of scatter in the initial yield response of the material. It is also worth noting that an error of 0.25 mm in measured crack length would lead to changes of about 10% in both K_r and S_r for a given load, so that the experimental curve is very sensitive to the crack length. The overall conclusion from Fig. 7 is that too much reliance should not be placed on limited finite-element or experimental data in the intermediate load regime as numerical or experimental error, the choice of collapse load expression and scatter in material behaviour can lead to considerable variations in the results when plotted on the failure assessment diagram.

5. CONCLUSIONS

5.1 J-estimation schemes based on finite-element solutions for power-law hardening materials have been written in terms of the shape of the material stress–strain curve by using reference stress techniques. This removes the strong dependence of the schemes on the hardening parameters which otherwise have to be chosen to describe the stress–strain response.

5.2 The resulting estimation scheme has been used to derive a failure assessment curve for use with the CEGB failure assessment route. In general the failure assessment curve depends on geometry but a geometry independence has been obtained by making a simple approximation. It has been shown that compared to the original estimation scheme, the approximation typically leads to a reduction in predicted load bearing capacity of 5% in the post-yield fracture region for some standard test specimen geometries. Similar differences may be expected for components so that making the approximation does not seem an unreasonable penalty for obtaining a geometry-independent assessment curve given the alternative of requiring the use of detailed J solutions for specific geometries.

5.3 The present reference stress based assessment curve depends on the full stress–strain curve as opposed to the recent suggestion of Milne [6] which depends only on the ratio of ultimate strength to yield strength. It has been shown that the two approaches are similar for materials with a low ratio of ultimate to yield stress or materials with a high initial hardening rate (specifically, the strain at a stress 30% between yield and ultimate should be only a small multiple (4, say) of the elastic strain). However, the approach of Milne is likely to be unconservative for materials which exhibit large strains at stresses not much greater than the yield stress yet have a high ratio of ultimate to yield strength.

5.4 In the post-yield fracture region, numerical or experimental error, the choice of limit load expression and scatter in material yield properties can lead to considerable variation in results plotted on the failure assessment diagram.

Acknowledgement—This paper is published by permission of the Central Electricity Generating Board.

REFERENCES

[1] R. P. Harrison, K. Loosemoore, I. Milne and A. R. Dowling, Assessment of the Integrity of Structures Containing Defects, *CEGB Report* R/H/R6–Rev. 2 (1980).
[2] F. M. Burdekin, The PD6493 Approach to Significance of Defects, Conference on Fitness for Purpose Validation of Welded Constructions, The Welding Institute, London (1981).
[3] C. E. Turner, A J-based design curve. In *Advances in Elastic –Plastic Fracture Mechanics* (Edited by Larson). Applied Science (1980).
[4] V. Kumar and C. F. Shih, Fully plastic crack solutions, estimation scheme and stability analyses for the compact specimen, *ASTM-STP* **700**, 406–438 (1980).
[5] F. M. Burdekin, A. Cowan, I. Milne and C. E. Turner, Comparison of COD, R6 and J-contour Integral Methods of Defect Assessment, Modified to give Critical Flaw Sizes, Conference as [2].
[6] I. Milne, Failure assessment Diagrams and J Estimates: A Comparison for Ferritic and Austenitic Steels, *CEGB Report* RD/L/2208N81 (1982).
[7] N. L. Goldman and J. W. Hutchinson, Fully plastic crack problems: the centre-cracked strip under plane strain, *Int. J. Solids Structures* **11**, 575–591 (1975).
[8] C. F. Shih and J. W. Hutchinson, Fully plastic solutions and large scale yielding estimates for plane stress crack problems, *J. Engng Mat. Technology* **98**, 289–295 (1976).
[9] M. P. Ranaweera and F. A. Leckie, J Integrals for some crack and notch geometries, *Int. J. Fracture* **18**, 3–18 (1982).
[10] R. K. Penny and D. L. Marriott, *Design for Creep*. McGraw-Hill, New York (1971).
[11] J. R. Haigh and C. E. Richards, Yield Point Loads and Compliance Functions of Fracture Mechanics Specimens, *CEGB Report* RD/L/M461 (1974).
[12] M. Y. He and J. W. Hutchinson, The penny-shaped crack and the plane strain crack in an infinite body of power-law material, *J. Appl. Mech.* **48**, 830–840 (1981).
[13] A. G. Miller, Review of Limit Loads of Structures Containing Defects, *CEGB Report* TPRD/B/0093/N82 (1982).
[14] G. G. Chell, Elastic-plastic fracture mechanics, In *Developments in Fracture Mechanics* (Edited by G. G. Chell). Applied Science (1980).
[15] R. P. Harrison, K. Loosemore and I. Milne, Assessment of the Integrity of Structures Containing Defects, Supplement 1—Validation, CEGB Report R/H/R6 Supplement 1 (1979).
[16] D. S. Dugdale, Yielding of steel sheets containing slits, *J. Mech. Phys. Solids* **8**, 100–104 (1960).
[17] R. Bradford, Private Communication (1982).
[18] B. K. Neale and C. H. A. Townley, Comparison of elastic–plastic fracture mechanics criteria, *Int. J. Pres. Ves. Piping* **5**, 207–239 (1977).
[19] B. K. Neale, The influence of Side-Grooving on Pre-Cracked Charpy Specimens in Bending, *Int. J. Press. Ves. Piping* **10**, 375–398 (1982)-plus private communication of additional data (1982).

(*Received* 14 *March* 1983)